Solar Energy 256 (2023) 96–109

Contents lists available at ScienceDirect

Solar Energy

journal homepage: www.elsevier.com/locate/solener

Simplified analytical model to describe wind loads and wind-induced tracking deviations of heliostats

Kristina Blume [a,*], Marc Röger [b], Robert Pitz-Paal [c]

[a] German Aerospace Center (DLR), Institute of Solar Research, Karl-Heinz-Beckurts Str. 13, 52428 Jülich, Germany
[b] German Aerospace Center (DLR), Institute of Solar Research, Paseo de Almería 73, 04001 Almería, Spain
[c] German Aerospace Center (DLR), Institute of Solar Research, RWTH Aachen University, Chair of Solar Technology, Linder Höhe, 51147 Cologne, Germany

ARTICLE INFO

Keywords:
Solar tracker
Heliostat
Wind load
Tracking error
Analytical model

ABSTRACT

Wind-induced tracking deviations of heliostats can be analyzed through numerical simulations or experimental studies on a full-scale heliostat. However, these methods are relatively costly and often, simpler estimations are necessary and sufficient. One simpler approach is to use an analytical model that describes the wind-induced tracking deviations and which requires only a few input parameters that can be determined through straightforward measurements at the full-scale heliostat. Therefore, this paper presents the derivation of an analytical model and describes the development process in a detailed way to clarify the necessary assumptions and simplifications. For verification purposes, the developed model is furthermore applied to measurement data of a field study. It is shown that the results of the model application agree well with the expectations and that the measured heliostat response matches the predicted response well, provided the underlying assumptions of the model fully apply to the investigated heliostat. Overall, no unexplainable inconsistencies are identified and the results support the model well. Thus, a method is provided which allows the estimation and prediction of wind-induced tracking deviations with comparatively little effort. In addition, the developed model helps to identify and analyze those parameters that have the greatest impact on the wind-induced tracking deviations of different types of heliostats.

1. Introduction

Heliostats of a solar tower plant have the primary function to reflect the incident solar radiation on a desired aimpoint on the receiver. The necessary adjustment of the heliostats' orientation throughout the day, i.e. the tracking, must therefore be highly accurate. Yet, operational loads, in particular wind loads, can affect the tracking accuracy by inducing oscillations and causing misalignments of the concentrator that result in tracking deviations. Due to tracking deviations, the reflected beam does not reach its desired aimpoint on the receiver and the operation and performance of the solar tower plant can be affected. In particular those heliostats positioned at the far end of a heliostat field can make a strong impact. The far-field heliostats lack shielding effects of surrounding heliostats and are thus exposed to much stronger winds, leading to increased tracking deviations. At the same time, due to their large distance to the tower, the tracking deviations of far-field heliostats lead to larger movements of the reflected beam on the tower, thus to a stronger impact on the plant. As tracking deviations can affect the performance and operation of a solar tower plant, a method to estimate and predict wind-induced tracking deviations can help to optimize the plant. Moreover, it can help to optimize the design of a heliostat which has to withstand wind loads during operation to ensure a sufficient tracking accuracy while over-dimensioning must be avoided to keep the costs low.

In the past, wind-induced tracking deviations have been analyzed based on numerical simulations (Teufel et al., 2008; Vásquez Arango, 2016) or experimental investigations on the full-scale heliostat (Blume et al., 2020). However, both of these methods are relatively costly and often, simpler estimations are necessary and sufficient. One simpler approach is to use an analytical model that describes the wind-induced tracking deviations and which requires only a few input parameters that can be determined through straightforward measurements at the full-scale heliostat. In principal, the analytical model must describe the transmission of wind into an aerodynamic load (the aerodynamic side) and further the transmission of the load into a structural response (the structural side). Details about the aerodynamic and structural side will later be explained in Section 2. For structures such as buildings and trains, analytical models with varying complexity can be found in the literature, partly taking the aerodynamic side only into account

* Corresponding author.
E-mail address: kristina.blume@dlr.de (K. Blume).

https://doi.org/10.1016/j.solener.2023.03.055
Received 1 August 2022; Received in revised form 16 January 2023; Accepted 25 March 2023
Available online 8 April 2023

Nomenclature

$\overline{a}$	Mean component of variable a ([a])
A	Total concentrator area (m^2)
a	General variable ([a])
a'	Fluctuating component of variable a ([a])
a_i	Matrix entries $i = 1, 2, 3, 4$ (–)
C	Ratio of inverse concentrator stiffnesses (–)
c_L	Non-dimensional coefficient of general load component L (–)
$c_{M_{ax}}$	Moment coefficient about axis ax (–)
$c_{v,ax}$	Viscous damping coefficient related to axis ax (Nm s/rad)
f_e	Eigenfrequency (Hz)
J_{ax}	Moment of inertia about axis ax (kg m^2)
k^*_{ax}	Inverse concentrator stiffness about axis ax (rad/Nm)
k_{ax}	Concentrator stiffness about axis ax (Nm/rad)
l^*_{ax}	Characteristic length in inverse direction of axis ax (m)
l_{ax}	Characteristic length in direction of axis ax (m)
M_{ax}	Aerodynamic moment about axis ax (Nm)
S_u	PSD of longitudinal wind speed ((m/s)^2/Hz)
S_v	PSD of lateral wind speed ((m/s)^2/Hz)
S_w	PSD of vertical wind speed ((m/s)^2/Hz)
$S_{\Delta\delta_{ax}}$	PSD of wind-induced deviation (rad^2/Hz)
$S_{\Delta Track_{ax,wind}}$	PSD of wind-induced tracking deviation (rad^2/Hz)
S_{c_L}	PSD of general load coefficient (1/Hz)
$S_{c_{Max}}$	PSD of moment coefficient about axis ax (1/Hz)
$S_{M_{ax}}$	PSD of moment about axis ax ((Nm)^2/Hz)
$S_{M_{xh}M_{yh}}$	Co-spectrum between moments about x_h- and y_h-axis ((Nm)^2/Hz)
S_{uv}	Co-spectrum between longitudinal and lateral wind speed ((m/s)^2/Hz)
S_{uw}	Co-spectrum between longitudinal and vertical wind speed ((m/s)^2/Hz)
S_{vw}	Co-spectrum between lateral and vertical wind speed ((m/s)^2/Hz)
$Track_{ax}$	Total tracking deviation about axis ax (rad)
u	Longitudinal wind speed component (m/s)
u_{tot}	Total wind speed (m/s)
v	Lateral wind speed component (m/s)
w	Vertical wind speed component (m/s)
x_h	Horizontal concentrator axis (m)
y_h	Vertical concentrator axis (m)
z_h	Axis orthogonal to concentrator surface; Optical axis (m)
AOR	Axis of rotation
MDOF	Multiple degree of freedom
PSD	Power spectral density
SDOF	Single degree of freedom
α	Vertical angle of attack (rad,°)
β	Horizontal angle of attack (rad,°)
$\chi_{m,ax}$	Dynamic magnification factor related to axis ax (–)
$\ddot{\delta}_{ax}$	Second time derivative of wind-induced deviation (rad/s^2)
$\Delta Track_{ax,wind}$	Wind-induced tracking deviation about concentrator axis $ax = x_h, y_h$ (rad)
δ_{ax}	Wind-induced deviation about an arbitrary axis (rad)
$\dot{\delta}_{ax}$	First time derivative of wind-induced deviation (rad/s)
$\lvert\chi_{a,ax}\rvert^2$	Aerodynamic admittance function of moment about axis ax (–)
$\lvert\chi_{a,L}\rvert^2$	Aerodynamic admittance function of general load component L (–)
$\lvert\chi_{m,ax}\rvert^2$	Mechanical admittance function related to axis ax (–)
$\overline{\alpha}$	Elevation angle (°)
ρ	Air density (kg/m^3)
θ	Rotation angle between concentrator and AOR system (rad,°)
ξ	Damping ratio (–)

(e.g. Baker et al. (2004)) and partly including the structural side as well (e.g. Holmes (2015), Quinn et al. (2007), Dyrbye and Hansen (1999), Ruscheweyh (1982)). However, these models are not fully transferable to heliostats and their unique characteristics such as the varying orientation of the concentrator. Therefore, Vásquez Arango (2016) developed an analytical model for a heliostat to describe its wind-induced tracking deviations. Yet, parts of that model are still relatively complex as Vásquez Arango (2016) had results of a comprehensive simulation study available which he could use as input parameters for the analytical model.

Therefore, the main objective of this study is to derive and provide a simplified analytical model for which only commonly available or easy-to-determine input parameters are required. Moreover, the derivation of the model shall be described in a detailed way so that the necessary assumptions and limitations of the model become clear and transparent. Overall, through the development of a simplified analytical model, a method shall be provided based on which wind-induced tracking deviations can be estimated and predicted for different types of heliostats with comparatively little effort.

The development of the analytical model, also referred to as the model representation or simply the model, is described in Section 2. The model will be developed for a simple heliostat design which can then be transferred to more complex heliostat designs. Such adjustment of the model representation is exemplarily described in Section 3 for a pentagonal heliostat with two inclined linear actuators (Stellio type heliostat) and a rectangular heliostat with a pylon mounted gear drive and a linear actuator (T-type heliostat). An application of the model to measurement data of a field study is then described in Section 4 to discuss and verify the developed model. Lastly, for the practical use of the analytical model, Section 5 briefly describes the workflow and the determination of the required input parameters. Finally, a concluding summary is given in Section 6.

2. Derivation of analytical model

In this section, an analytical model will be developed to describe aerodynamic loads and wind-induced tracking deviations of heliostats. More specifically, the case of an isolated heliostat subject to the natural wind conditions will be considered. An application to heliostat fields is potentially possible and will be addressed later. Prior to developing the model, a few preliminary remarks and definitions will be introduced.

First, a heliostat coordinate system has to be defined which is shown in Fig. 1. The depicted system (x_h, y_h, z_h) is equivalent to the

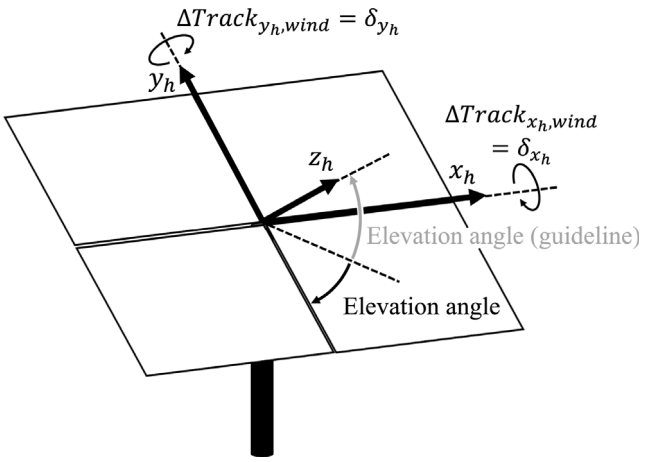

Fig. 1. Schematic of a heliostat with definition of the concentrator coordinate system and the elevation angle. Guideline refers to SolarPACES guideline (Röger et al., 2022).

concentrator coordinate system (CCS) as defined by the SolarPACES heliostat performance testing guideline (Röger et al., 2022). The x_h-axis is defined horizontally, the y_h-axis is defined vertically in the plane of the concentrator and the z_h-axis points away from the concentrator. Besides the concentrator coordinate system, Fig. 1 shows in black the definition of the elevation angle as used in this study (angle between the line that horizontally points away from the concentrator and the concentrator plane). Note that there is a second option to define the elevation angle, shown in gray (angle between the horizontal line and the concentrator normal, i.e. the z_h-axis), which is also often applied e.g. by the SolarPACES guideline. Both definitions can be easily converted.

As a second preliminary remark, the heliostat's tracking deviation shall be introduced. In general terms, the tracking deviation describes the angular deviation between the concentrator's actual orientation (i.e. the direction of its optical axis z_h) and its desired orientation (Sattler et al., 2020). While tracking deviations can occur due to many reasons such as the motor control system or wear of the gears (Heller, 2017), which altogether lead to a total tracking deviation $Track_{ax}$, this study focuses specifically and only on wind-induced tracking deviations. As these are additional tracking deviations that only occur under certain wind conditions, they are termed $\Delta Track_{ax,wind}$ and are typically given in the unit mrad. The subscript ax refers to the specific axes about which the angular deviations are defined which, in this study, will be the horizontal (x_h) and vertical (y_h) concentrator axes. Note that for simplicity of notation, $\Delta Track_{x_h,wind}$ and $\Delta Track_{y_h,wind}$ will be substituted by δ_{x_h} and δ_{y_h} at some points during this paper.

As a third preliminary remark, the approach and method to model the wind-induced tracking deviation shall be introduced. In principal, the heliostat's wind-induced tracking deviation ($\Delta Track_{ax,wind}$) is caused by an aerodynamic moment (M_{ax}) which in turn is induced by the approaching wind, composed of the longitudinal, lateral and vertical wind speeds (u, v and w). Based on this understanding, a model representation of $\Delta Track_{ax,wind}$ will be derived in two steps. (1) First, the transmission of the approaching wind u, v, w into a corresponding aerodynamic moment M_{ax} will be modeled which is explained in the following Section 2.1. This part will also be termed the modeling of the aerodynamic side. (2) Second, the transmission of the aerodynamic moment M_{ax} into a corresponding wind-induced response of the heliostat δ_{ax} will be modeled. Note that the term response and the variable δ_{ax} are used to describe a rotation of the concentrator about an arbitrary axis ax. The desired tracking deviation $\Delta Track_{ax,wind}$ is a special case of the response and describes a concentrator rotation specifically about the two concentrator axes $ax = x_h, y_h$. The modeling of the tracking deviation or more generally of the response will also be termed the modeling of the structural side and is presented in Section 2.2. In addition to the decomposition into an aerodynamic and a structural side, the entire modeling process will furthermore be divided into describing (a) mean components and (b) fluctuating components with zero mean for all quantities, i.e. wind, load and response. The mean component of a quantity a will be stated as $\overline{a}$ and the fluctuating component as a'. Such decomposition into a mean and fluctuating component is related to the characteristics of the natural wind. Close to the ground, the interaction of the wind and the earth's surface creates eddies of different sizes, known to be turbulence (Stull, 1988). Within the turbulent wind flow, the wind speed varies in time with different strengths. In fact, it was found that wind speed variations corresponding to time periods of approximately 10 min to 2 h are very small (van der Hoven, 1957). Therefore, they can be treated as quasi-stationary which in turn allows the aforementioned decomposition into a static, mean component and into a dynamic, fluctuating component. In conclusion, the mean component of each quantity of the following model representation describes the static behavior while the fluctuating component describes the dynamic behavior due to the turbulence of the natural wind.

The preceding explanations describe the general process to develop the model representation. More specific assumptions and simplifications necessary to develop the model will be introduced during the following Sections 2.1 and 2.2. These simplifications and assumptions will also later be summarized and further discussed in Section 2.3.

Lastly, note that the following model representation takes into account only those dynamic effects which are related to the natural turbulence of the wind while effects such as vortex shedding or aerodynamic damping are not included. Yet, the model representation can be adjusted in future to account for these effects as well.

2.1. Model representation of the aerodynamic moment

The following development of a model representation is partly based on the explanations and derivations in Ruscheweyh (1982), Quinn et al. (2007) and Baker et al. (2004), here adopted to the specific case of a heliostat.

The underlying principle of modeling the aerodynamic moment is to make use of normalized moment coefficients which are of the general form $c_M = M/(\frac{\rho}{2}u^2Al)$ where M is the dimensional moment, ρ is the air density, u is the wind speed, A is the heliostat's area and l is a characteristic length of the heliostat. Moment coefficients are for example determined through wind tunnel or field studies where a heliostat is exposed to certain wind conditions, the moment on the heliostat is measured, and finally transformed into a moment coefficient. More details about the moment coefficients needed for the final analytical model will be given later in Section 2.3. At this point, it is important to understand that a moment coefficient is a single value which encapsulates the entire transmission process of a certain wind condition into the corresponding acting moment on the heliostat. In particular, effects such as a wind speed gradient over the height above ground, which can cause moments on the heliostat, are implicitly included in the moment coefficient.

In the framework of this study, the aerodynamic moment about the heliostat's vertical (M_{y_h}) and horizontal concentrator axis (M_{x_h}) is of concern as these two moments are the cause for the wind-induced tracking deviations. Due to the turbulent nature of the wind, the instantaneous aerodynamic moment varies in time and can be expressed for either axis $ax = x_h, y_h$ as

$$M_{ax}(t) = \frac{\rho}{2}u_{tot}^2(t)Al_{ax}^*c_{M_{ax}}\left(\alpha(t),\beta(t)\right) \tag{1}$$

where ρ is the air density, A is the concentrator surface area and l_{ax}^* is the concentrator's characteristic length. In case of the moment about the x_h-axis, the characteristic length is typically defined in y_h-direction,

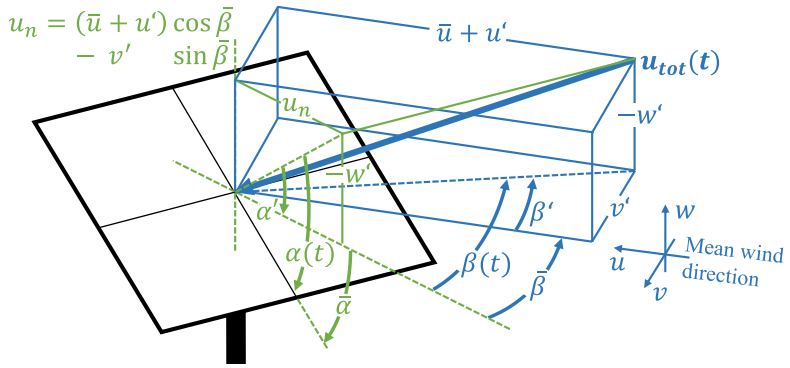

Fig. 2. Schematic of the instantaneous wind approaching a heliostat. Blue coordinate system represents the natural wind system in which coordinate u is aligned with the mean wind direction. (For interpretation of the references to color in this figure legend, the reader is referred to the web version of this article.)

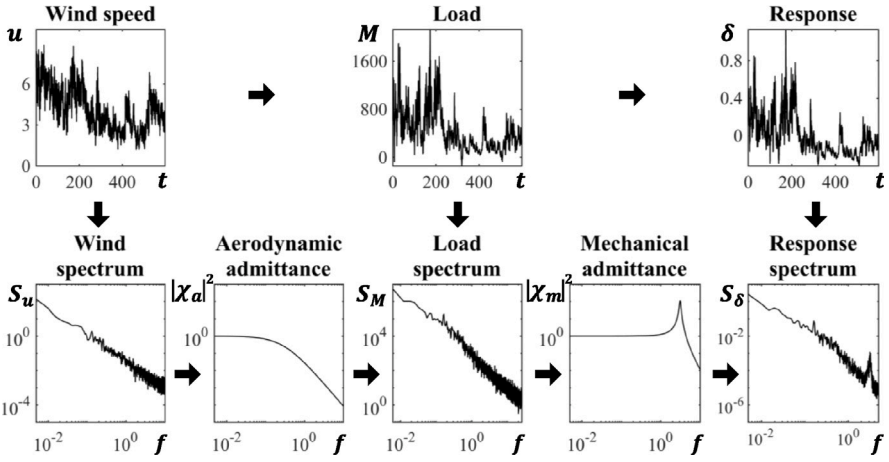

Fig. 3. Schematic of Davenport's spectral approach to describe wind-induced fluctuating aerodynamic loads on a structure as well as the structure's dynamic response (based on Davenport, 1964).

described by the variable l_{y_h}. For simplicity of notation, the variable l_{y_h} is substituted by $l^*_{x_h}$. The same applies to the moment about the y_h-axis with a characteristic length $l_{x_h} = l^*_{y_h}$. Note that the exact definition of the characteristic length can be found in the respective study from which the moment coefficients are taken. Furthermore, in Eq. (1) $u_{tot}(t)$ denotes the instantaneous total wind speed at elevation axis height as indicated in Fig. 2. The blue coordinate system in Fig. 2 represents the so called natural wind system. It is oriented parallel to the ground and the u-component is aligned with the mean wind direction. Within the natural wind system, the total wind speed is decomposed into a mean component in longitudinal direction ($\bar{u}$) and into fluctuating components in longitudinal, lateral and vertical direction (u', v', w') with zero mean (Dyrbye and Hansen, 1999). Hence, the total wind speed can be approximated as follows when neglecting the square of the fluctuating wind speed components:

$$u_{tot}(t)^2 = \left(\bar{u} + u'\right)^2 + v'^2 + w'^2 \approx \bar{u}^2 + 2\bar{u}u' \tag{2}$$

Lastly, in Eq. (1) $c_{M_{ax}}(t)$ represents the instantaneous non-dimensional moment coefficient which is a function of the instantaneous angles of attack $\alpha(t)$ and $\beta(t)$ as defined in Fig. 2.

Note that in case of heliostats, the mean vertical angle of attack $\bar{\alpha}$ is determined by the elevation angle and therefore, the instantaneous angle $\alpha(t)$ as well as the fluctuating component α' must be defined accordingly. With respect to the differently oriented wind coordinate system (blue in Fig. 2), this leads to a rather complex definition of $\alpha(t)$ and α' as depicted in Fig. 2 and evaluated in more detail later.

The instantaneous aerodynamic moment coefficient $c_{M_{ax}}(\alpha(t), \beta(t))$ can be further developed by applying a Taylor approximation up to the first order which leads to

$$\begin{aligned} c_{M_{ax}}\left(\alpha(t), \beta(t)\right) \approx \bar{c}_{M_{ax}} &+ \left.\frac{\partial c_{M_{ax}}}{\partial \alpha}\right|_{\bar{\alpha},\bar{\beta}} \left(\alpha(t) - \bar{\alpha}\right) \\ &+ \left.\frac{\partial c_{M_{ax}}}{\partial \beta}\right|_{\bar{\alpha},\bar{\beta}} \left(\beta(t) - \bar{\beta}\right) \end{aligned} \tag{3}$$

in which $\left.\frac{\partial c_{M_{ax}}}{\partial \alpha}\right|_{\bar{\alpha},\bar{\beta}}$ and $\left.\frac{\partial c_{M_{ax}}}{\partial \beta}\right|_{\bar{\alpha},\bar{\beta}}$ denote the partial derivatives of the aerodynamic moment coefficient with respect to the angles of attack, evaluated at the mean angles of attack. The notation of the evaluation point will be removed in the following for simplicity. In Eq. (3), furthermore $\left(\alpha(t) - \bar{\alpha}\right)$ and $\left(\beta(t) - \bar{\beta}\right)$ define the fluctuating angles of attack α' and β', respectively. While β' can be approximated as follows when assuming that $u', v' \ll \bar{u}$

$$\beta' = \beta(t) - \bar{\beta} = \arctan\left(\frac{v'}{\bar{u} + u'}\right) \approx \frac{v'}{\bar{u}} \tag{4}$$

the description of the fluctuating angle of attack α' is rather complex due to aforementioned reasons. Using the auxiliary variable u_n as defined in Fig. 2, α' can be expressed as

$$\begin{aligned} \alpha' &= \alpha(t) - \bar{\alpha} = \arctan\left(\frac{-w'}{u_n}\right) \\ &= \arctan\left(\frac{-w'}{(\bar{u} + u')\cos\bar{\beta} - v'\sin\bar{\beta}}\right) \end{aligned} \tag{5}$$

and cannot easily be approximated in a general way. However, for rather small $\bar{\beta}$ it is reasonable to assume that $(\bar{u}+u')\cos\bar{\beta} \gg v'\sin\bar{\beta}$ and in this case, α' can be approximated to $\frac{-w'}{\bar{u}}$ when again assuming that $u', w' \ll \bar{u}$. Substituting aforementioned α'-approximation and Eq. (4) into Eq. (3) and further substituting Eqs. (2) and (3) into Eq. (1) while

again neglecting the square of the fluctuating wind speed components, the instantaneous aerodynamic moment in non-dimensional form reads

$$c_{M_{ax}}(t) = \frac{M_{ax}(t)}{\frac{\rho}{2}\overline{u}^2 A l^*_{ax}} = \underbrace{\overline{c}_{M_{ax}}}_{\substack{mean\\component}} + \underbrace{2\,\overline{c}_{M_{ax}}\frac{u'}{\overline{u}} + \frac{\partial c_{M_{ax}}}{\partial\beta}\frac{v'}{\overline{u}} + \frac{\partial c_{M_{ax}}}{\partial\alpha}\frac{-w'}{\overline{u}}}_{\substack{fluctuating\\component}} \tag{6}$$

In Eq. (6), the first summand represents the mean component of the non-dimensional aerodynamic moment ($\overline{c}_M$) while the remaining summands represent the fluctuating component (c'_M). At this point, it must be outlined that the fluctuating aerodynamic moment is not only varying with time but is also a function of the frequency f. This effect is related to the coexistence of different size eddies in the turbulent wind flow where small eddies and their related wind speed fluctuations correspond to high frequencies and vice versa. Such eddies that are small compared to the structure only cover and act on a small area of the surface simultaneously, thus their spatial correlation is reduced (Petersen and Werkle, 2017; Dyrbye and Hansen, 1999). As a consequence, they are less effective in inducing loads on a structure. This effect is accounted for by the so called aerodynamic admittance function which is defined in frequency domain and tends towards unity for very low frequencies and decreases towards high frequencies. Therefore, the fluctuating component of the aerodynamic moment is best modeled in frequency domain which is also known as the spectral approach (Holmes, 2015) that was firstly introduced by Davenport (1961). Fig. 3 shows a schematic of Davenport's spectral approach where the power spectral density S, also simply termed spectrum, of the fluctuating moment is linked to the wind spectrum by the aerodynamic admittance. Fig. 3 furthermore depicts the transformation of the load spectrum into the response spectrum which will be explained later in Section 2.2.

Following the spectral approach, the description of c'_M given in Eq. (6) must be transformed from time into frequency domain where the aerodynamic admittance function $|\chi_a|^2$ can then be applied. An equivalent expression in frequency domain in terms of the power spectral density (PSD) can be derived by firstly squaring and then averaging (Davenport, 1967) the expression of c'_M as follows:

$$\begin{aligned}\overline{\left(c'_{M_{ax}}\right)^2} &= \overline{\left(2\overline{c}_{M_{ax}}\frac{u'}{\overline{u}} + \frac{\partial c_{M_{ax}}}{\partial\beta}\frac{v'}{\overline{u}} + \frac{\partial c_{M_{ax}}}{\partial\alpha}\frac{-w'}{\overline{u}}\right)^2}\\ &= 4\overline{c}^2_{M_{ax}}\frac{\overline{u'^2}}{\overline{u}^2} + \left(\frac{\partial c_{M_{ax}}}{\partial\beta}\right)^2\frac{\overline{v'^2}}{\overline{u}^2} + \left(\frac{\partial c_{M_{ax}}}{\partial\alpha}\right)^2\frac{\overline{w'^2}}{\overline{u}^2}\\ &\quad + 4\overline{c}_{M_{ax}}\left(\frac{\partial c_{M_{ax}}}{\partial\beta}\right)\frac{\overline{u'v'}}{\overline{u}^2} + 4\overline{c}_{M_{ax}}\left(\frac{\partial c_{M_{ax}}}{\partial\alpha}\right)\frac{\overline{-u'w'}}{\overline{u}^2}\\ &\quad + 2\left(\frac{\partial c_{M_{ax}}}{\partial\alpha}\right)\left(\frac{\partial c_{M_{ax}}}{\partial\beta}\right)\frac{\overline{-v'w'}}{\overline{u}^2}\end{aligned} \tag{7}$$

The final expression of Eq. (7) can be directly translated into the power spectral density $S_{c_M}(f)$. When furthermore applying the aerodynamic admittance function $|\chi_a(f)|^2$, the complete model representation of c'_M in frequency domain in terms of its PSD reads

$$\begin{aligned}S_{c_{Max}} = |\chi_{a,ax}|^2 \Bigg[&4\overline{c}^2_{M_{ax}}\frac{S_u}{\overline{u}^2} + \left(\frac{\partial c_{M_{ax}}}{\partial\beta}\right)^2\frac{S_v}{\overline{u}^2} + \left(\frac{\partial c_{M_{ax}}}{\partial\alpha}\right)^2\frac{S_w}{\overline{u}^2}\\ &+ 4\overline{c}_{M_{ax}}\left(\frac{\partial c_{M_{ax}}}{\partial\beta}\right)\frac{S_{uv}}{\overline{u}^2} - 4\overline{c}_{M_{ax}}\left(\frac{\partial c_{M_{ax}}}{\partial\alpha}\right)\frac{S_{uw}}{\overline{u}^2}\\ &- 2\left(\frac{\partial c_{M_{ax}}}{\partial\alpha}\right)\left(\frac{\partial c_{M_{ax}}}{\partial\beta}\right)\frac{S_{vw}}{\overline{u}^2}\Bigg]\end{aligned} \tag{8}$$

In Eq. (8), the variables S_u, S_v and S_w denote the power spectral densities of the fluctuating wind speed components u', v' and w', respectively. In addition, the variables S_{uv}, S_{uw} and S_{vw} represent the co-spectra between the fluctuating wind speed components u' and v', u' and w' and v' and w', respectively. To reduce the complexity of the model representation, the co-spectra are often neglected.

In conclusion, the total aerodynamic moment acting on a heliostat is composed of a mean and a fluctuating component which can be modeled as follows. The mean component is calculated through the well known mean aerodynamic moment coefficient by

$$\overline{M}_{ax} = \frac{\rho}{2}\overline{u}^2 A l^*_{ax}\overline{c}_{M_{ax}} \tag{9}$$

while the fluctuating component is determined as follows when considering the simplified model representation, i.e. neglecting the co-spectra:

$$\begin{aligned}S_{M_{ax}} &= \left(\frac{\rho}{2}\overline{u}^2 A l^*_{ax}\right)^2 S_{c_{Max}}\\ &= \left(\frac{\rho}{2}\overline{u}^2 A l^*_{ax}\right)^2|\chi_{a,ax}|^2\left[4\overline{c}^2_{M_{ax}}\frac{S_u}{\overline{u}^2} + \left(\frac{\partial c_{M_{ax}}}{\partial\beta}\right)^2\frac{S_v}{\overline{u}^2} + \left(\frac{\partial c_{M_{ax}}}{\partial\alpha}\right)^2\frac{S_w}{\overline{u}^2}\right]\end{aligned} \tag{10}$$

Note that aforementioned model representation of the fluctuating component does not only apply to the aerodynamic moment but can be more generally applied to any load component such as the drag or the lift force. In that case, the subscript M_{ax} is simply replaced by the respective load component. If the desired load component is a force rather than a moment, furthermore the characteristic length l^* needs to be removed from Eq. (10).

Lastly, note that the power spectral density $S(f)$ of a signal with zero mean, here the fluctuating aerodynamic moment, can be translated into the signal's variance σ^2 through integration as follows

$$\sigma^2 = \int S(f)\,df \tag{11}$$

2.2. Model representation of the wind-induced tracking deviation

From the model representation of the aerodynamic moment, the heliostat's wind-induced response and furthermore the desired tracking deviation can finally be determined. Analogously to the aerodynamic moment, the wind-induced response can in principal be divided into a mean and a fluctuating component. Moreover, the fluctuating or dynamic response can be divided into a background and a resonant component. The background response comprises oscillations that closely follow the fluctuating load, caused by a direct response of the heliostat to the fluctuating load. In addition, the fluctuating wind load can excite eigenfrequencies of the heliostat which leads to additional oscillations that are superimposed to the background response. Such behavior is termed the resonant response. Note that each (excited) eigenfrequency is associated with a characteristic modal motion, i.e. the mode shape (de Silva, 2005), which can for example represent torsion (torsional modes) or deformation (bending modes). Moreover, rigid body modes can appear if the structure under investigation is unrestrained in one degree of freedom. Typically, structures are restrained in all degrees of freedom. Yet, in case of a heliostat, the connection of the concentrator to the pylon can be considered of low stiffness and in that case so called approximate rigid body modes can appear which will be prominent at low frequencies (de Silva, 2005).

To develop a model representation of the heliostat's mean and fluctuating response, the principles of a mass–spring–damper system are considered. In reality, a heliostat is a multiple degree of freedom (MDOF) system which is rather complex to model. However, under the following assumptions, the heliostat's response to wind load can be modeled based on the principles of a single degree of freedom (SDOF) system. The assumptions are that (1) the pylon is rigid and no oscillations (of the pylon) are induced by the wind; (2) the connection of the concentrator to the pylon is of low stiffness and oscillations of the concentrator about certain axes of rotation (AORs) can be induced; (3) the AORs are orthogonal; (4) the AORs are identical to the concentrator axes (x_h, y_h, z_h). Fig. 4 depicts a schematic of the

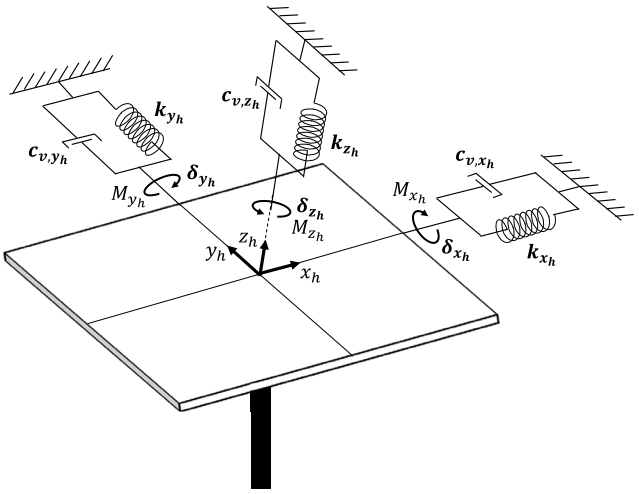

Fig. 4. Schematic of a heliostat mass–spring–damper system where the heliostat's axes of rotation are identical to the concentrator axes (x_h, y_h, z_h).

underlying mass–spring–damper system where the AORs are those axes to which the spring–damper combinations are related. The spring–damper combinations represent torsional components (torsional spring and torsional viscous damper), i.e. they react to a moment about the respective AOR. Note that the depicted heliostat model is the most simple system that can be defined. In this system, the concentrator is, in principle, the only rotatable part while additional components such as the drives are not considered. For such simple system, the principle axes of inertia are expected to coincide with the concentrator axes. Then, the wind-induced response about the concentrator x_h-, y_h- and z_h-axis can be modeled as three independent SDOF systems as follows.

The response of a mass–spring–damper system is described through differential equations of motion which can be derived by applying Newton's second law to the system under investigation (Kelly, 2012). Based on the schematic in Fig. 4, Newton's second law can be applied to the heliostat system. The second law states that the effective forces are equal to the external forces (Kelly, 2012). The effective force or moment is described by the moment of inertia J multiplied by the angular acceleration $\ddot{\delta}$ (Kelly, 2012). The external moments result from the spring and viscous damper and furthermore include the externally applied moment M. The moment created by the spring is described by the spring stiffness k and the angular displacement δ (Kelly, 2012). The damping moment, when assuming viscous damping, is described by the viscous damping coefficient c_v and the angular velocity $\dot{\delta}$ (Kelly, 2012).

Under consideration of aforementioned moments, a moment equation is developed about either axis of the heliostat. Regarding the external moments that are applied to a heliostat, the natural wind does not induce a significant moment about the z_h-axis as the concentrator is a rather thin object and the area exposed to the wind is small in this direction. Nevertheless, for completeness, the external moment M_{z_h} is included in the following moment equation and will be neglected later. Further note that due to expecting the principal axes to coincide with the concentrator axes, no products of inertia but simply the moments of inertia have to be considered, i.e. the inertia matrix is diagonal. Then, the moment equations about either axis read in matrix notation:

$$\begin{pmatrix} J_{x_h} & 0 & 0 \\ 0 & J_{y_h} & 0 \\ 0 & 0 & J_{z_h} \end{pmatrix} \begin{pmatrix} \ddot{\delta}_{x_h} \\ \ddot{\delta}_{y_h} \\ \ddot{\delta}_{z_h} \end{pmatrix} + \begin{pmatrix} c_{v,x_h} & 0 & 0 \\ 0 & c_{v,y_h} & 0 \\ 0 & 0 & c_{v,z_h} \end{pmatrix} \begin{pmatrix} \dot{\delta}_{x_h} \\ \dot{\delta}_{y_h} \\ \dot{\delta}_{z_h} \end{pmatrix} + \begin{pmatrix} k_{x_h} & 0 & 0 \\ 0 & k_{y_h} & 0 \\ 0 & 0 & k_{z_h} \end{pmatrix} \begin{pmatrix} \delta_{x_h} \\ \delta_{y_h} \\ \delta_{z_h} \end{pmatrix} = \begin{pmatrix} M_{x_h} \\ M_{y_h} \\ M_{z_h} \end{pmatrix} \tag{12}$$

Eq. (12) clarifies that the motions about the three AORs, here equivalent to the concentrator axes, are uncoupled. In an uncoupled case, the system behaves as an SDOF system in each respective direction, i.e. the motion about each axis can be modeled as an SDOF system. For an SDOF system, the so called dynamic magnification factor χ_m can be described by

$$\chi_m(f) = \frac{1}{\sqrt{\left(1 - \left(\frac{f}{f_e}\right)^2\right)^2 + \left(2\xi\frac{f}{f_e}\right)^2}} \tag{13}$$

in which f_e denotes the eigenfrequency and ξ the damping ratio (Kelly, 2012). The magnification factor accounts for the amplifying effect of the eigenfrequencies and allows to model the amplitude of the dynamic response $\hat{\delta}'$. The square of the magnification factor is also termed the mechanical admittance function which links the spectrum of the wind load to the response spectrum as indicated in Fig. 3. Finally, the mean response $\overline{\delta}$ and the amplitude of the dynamic response $\hat{\delta}'$ can be described by

$$\begin{aligned} \overline{\delta}_{ax} &= \frac{1}{k_{ax}}\overline{M}_{ax} = k^*_{ax}\overline{M}_{ax} \\ \hat{\delta}'_{ax} &= \frac{1}{k_{ax}}\widehat{M}'_{ax}\chi_{m,ax}(f) = k^*_{ax}\widehat{M}'_{ax}\chi_{m,ax}(f) \end{aligned} \tag{14}$$

where k^*_{ax} represents the inverse stiffness $1/k_{ax}$ and $\widehat{M}'_{ax}$ denotes the amplitude of the fluctuating aerodynamic moment.

As the magnification factor χ_m or the mechanical admittance function $|\chi_m|^2$ is a function of the frequency f, the dynamic response is best modeled in frequency domain, as proposed by the spectral approach, and its power spectral density reads

$$S_{\delta_{ax}}(f) = (k^*_{ax})^2 S_{M_{ax}} |\chi_{m,ax}|^2 \tag{15}$$

where $S_{M_{ax}}$ is the spectrum of the aerodynamic moment. At this point, it shall be emphasized that Eq. (15) describes the *total* dynamic response. As explained earlier, the total dynamic response can be further divided into a background and a resonant component where the background component is often considered to be the most dominant component (Holmes, 2015). In fact, this could be verified for a Stellio heliostat by Blume et al. (2020). Therefore, it can often be considered sufficient to model the background response only. Then, the model representation simplifies further. As the background response is known to closely follow the wind load, it becomes clear that the background spectrum can be determined simply by multiplying $(k^*_{ax})^2$ and $S_{M_{ax}}$ while neglecting the mechanical admittance function $|\chi_{m,ax}|^2$. Hence, the complexity of the model is reduced. In turn, only when intending to model the resonant response, the mechanical admittance function must be applied. In that case, note that the modeled resonant response will account for the excitation of only one eigenmode for each axis due to modeling the heliostat response by means of SDOF systems. Hence, the total resonant response as derived through the here developed model will consist of three eigenmodes that describe rotational approximate rigid body modes about the three depicted axes in Fig. 4, i.e. the AORs or the concentrator axes.

Finally, the desired wind-induced tracking deviations are equal to the modeled response about the x_h- and y_h-axis and can therefore be described as follows. The mean tracking deviation $\overline{\Delta Track}_{ax,wind} = \overline{\delta}_{ax}$ with $ax = x_h, y_h$ is described by

$$\overline{\Delta Track}_{ax,wind} = k^*_{ax}\overline{M}_{ax} = k^*_{ax}\frac{\rho}{2}\overline{u}^2 A l^*_{ax}\overline{c}_{M_{ax}} \tag{16}$$

The fluctuating tracking deviation $\Delta Track'_{ax,wind} = \delta'_{ax}$ with $ax = x_h, y_h$ is described through its power spectral density $S_{\Delta Track_{ax,wind}}$ as follows:

$$\begin{aligned} S_{\Delta Track_{ax,wind}}(f) &= (k^*_{ax})^2 \; S_{M_{ax}}(f) \; |\chi_{m,ax}(f)|^2 \\ &= (k^*_{ax}\frac{\rho}{2}\overline{u}^2 A l^*_{ax})^2 \; S_{c_{M_{ax}}}(f) \; |\chi_{m,ax}(f)|^2 \\ &= (k^*_{ax}\frac{\rho}{2}\overline{u}^2 A l^*_{ax})^2 \; |\chi_{a,ax}(f)|^2 \; |\chi_{m,ax}(f)|^2 \\ &\quad \left[4\,\overline{c}^2_{M_{ax}}\frac{S_u(f)}{\overline{u}^2} + \left(\frac{\partial c_{M_{ax}}}{\partial\beta}\right)^2 \frac{S_v(f)}{\overline{u}^2} + \left(\frac{\partial c_{M_{ax}}}{\partial\alpha}\right)^2 \frac{S_w(f)}{\overline{u}^2}\right] \end{aligned} \tag{17}$$

In conclusion, the wind-induced tracking deviation, consisting of a mean and a fluctuating component, is fully described by Eqs. (16) and (17). It shall be emphasized that the response modeling according to aforementioned equations is valid for those types of heliostats where the AORs are identical to the concentrator axes (assumption (4)). If this assumption is not valid, the model representation can be adjusted as exemplarily presented for two different types of heliostats in Section 3.

2.3. Simplifications and limitations of the model representation

The main underlying simplification of the developed model representation is a linearization of the wind speed, i.e. neglecting the square of the fluctuating wind speed components. The linearization is necessary to derive a reasonably simple model and is justified by the underlying fundamental aspect that the fluctuating wind speed component is typically smaller than the mean wind speed component. Considering this, the model representation is generally the more valid the smaller the turbulence intensity,[1] i.e. the weaker the wind speed fluctuations are compared to the mean wind speed. As the turbulence intensity varies for different heights above ground, smaller heliostats (exposed to stronger turbulence) can in principal be more affected by the applied simplifications. At the same time, heliostat moment coefficients typically account for an impact of the turbulence intensity and can partly counteract the effect. Due to a further necessary simplification, the applicability of the model is in some cases limited to small wind angles of attack $\overline{\beta}$, i.e. if the term related to the derivative $(\frac{\partial c_M}{\partial \alpha})$ is non-negligible. Otherwise, if the $(\frac{\partial c_M}{\partial \alpha})$-related term is negligible, the model applicability is unlimited with respect to $\overline{\beta}$. Aforementioned simplifications entail the main and strict (potential) limitations of the developed model as these simplifications cannot easily be avoided. Nevertheless, the simplifications are reasonable and a general limitation of the model is not expected.

At the current stage of development, additional yet non-strict limitations of the model applicability arise from the assumptions that the heliostat's pylon is rigid, that the axes of rotation are orthogonal and that the axes of rotation are identical to the concentrator axes. In particular the latter assumption is not mandatory but the model can, in principal, be extended and transformed between different axes, as exemplarily shown in Section 3. Even though the model representation becomes more complex if aforementioned assumptions are not fully valid, strict limitations do not arise. Also at the current stage of development, the applicability of the model is, strictly speaking, limited to the initially defined application case of a single heliostat subject to the natural wind conditions. For heliostat fields, the wind conditions can be significantly different (different wind spectra, increased turbulence intensity) and the moment coefficients of in-field heliostats may not be exactly equal to those of isolated heliostats. At the same time, aforementioned parameters are input parameters to the model representation so an application of the model to heliostat fields is, in principal, possible by simply exchanging the input parameters. However, it must be carefully evaluated in future if the underlying simplifications and assumptions are still (reasonably) valid for heliostat fields as the turbulence intensity can be increased and the wind speed fluctuations may therefore not be sufficiently smaller than the mean wind speed anymore.

On a final note, the model's dependency on the moment coefficients shall be addressed. As mentioned earlier, moment coefficients can be determined in wind tunnel or field studies by exposing a heliostat to certain wind conditions. The resulting moment coefficients are then, strictly speaking, tied to the specific wind conditions as well as to the specific heliostat type investigated in the study. For most accurate results of the analytical model, it is therefore advised to use moment coefficients determined for the particular type of heliostat and the particular wind conditions to be investigated. This aspect can potentially reduce the ease of use of the model. On the other hand, moment coefficients for a particular heliostat may be readily available from wind tunnel pre-studies which are often performed during the design process of the heliostat. Furthermore, moment coefficients can be, to a certain degree, transferable between heliostat types and wind conditions if a couple of key parameters are similar (e.g. turbulence intensity, concentrator aspect ratio). More information on the key parameters and on heliostat moment coefficients in general can be found for example in Blume et al. (2023) and Emes et al. (2021, 2019).

[1] For a certain period of time, the turbulence intensity is defined as the wind speed's standard deviation compared to the mean wind speed. It is therefore a measure of the strength of wind speed fluctuations in relation to the mean wind speed.

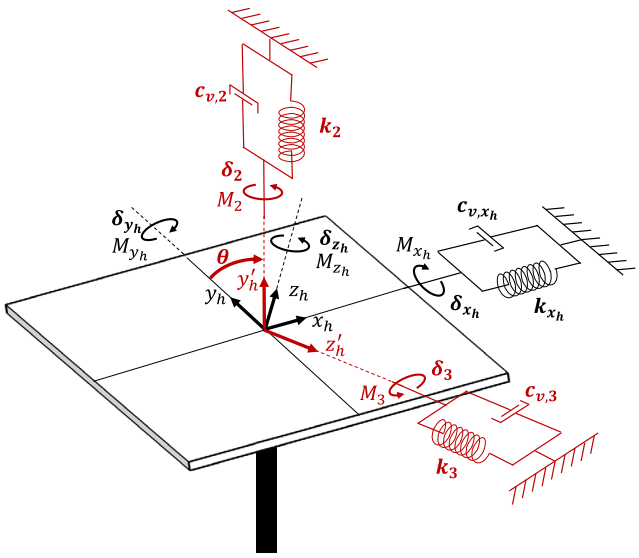

Fig. 5. Schematic of the mass–spring–damper system of a T-type heliostat. The expected axes of rotation (red) are rotated about the x_h-axis compared to the concentrator axes (black). (For interpretation of the references to color in this figure legend, the reader is referred to the web version of this article.)

3. Adjustment of analytical model

The axes of rotation (AORs) are those axes about which a heliostat is to a certain degree free to rotate and to which the spring–damper combinations are related. For many heliostat types, the AORs can be assumed to coincide with the tracking axes, i.e. those axes about which the drives adjust the concentrator. Note that in the SolarPACES guideline, the tracking axes can be found in the context of the heliostat axis coordinate system (ACS). As the tracking axes do not necessarily coincide with the concentrator axes (x_h, y_h, z_h), the previous assumption (4) is not valid and the model representation must be adjusted. This is exemplarily explained for two different types of heliostats in the following, i.e. (1) a rectangular T-type heliostat with a pylon mounted gear drive and a linear actuator and (2) a pentagonal heliostat with two inclined linear actuators.

3.1. T-type heliostat

The T-type heliostat considered in this context has a rectangular concentrator shape and contains a linear actuator and a pylon mounted gear drive. One example for such type of heliostat is the 14 m^2 HelFer heliostat, developed and manufactured by Kraftanlagen Energies & Services GmbH together with Heidelberger Druckmaschinen AG, as later shown in Fig. 8. For such T-type heliostat, a schematic of the mass–spring–damper system is shown in Fig. 5. As the linear actuator

is installed in such way that it adjusts the concentrator about the horizontal concentrator axis, the x_h-axis (shown in black) is assumed to be one axis of rotation. The gear drive is attached to the top of the pylon and adjusts the concentrator about the pylon axis which is therefore expected to be the second axis of rotation 2 (shown in red). In relation to the pylon axis, the concentrator y_h-axis is inclined according to the elevation angle. The third axis of rotation 3 (shown in red) is expected to horizontally point away from the concentrator. Together, the axes $x_h, 2, 3$ constitute the AORs. For the here considered T-type heliostat, the rotatable part of the system is a combination of the concentrator, the drives and all necessary reinforcements and fixations. For this combined system, the principal axes of inertia are assumed to be approximately equal to the axes $x_h, 2, 3$, i.e the AORs, and the equations of motion can then be described as follows:

$$\begin{pmatrix} J_{x_h} & 0 & 0 \\ 0 & J_2 & 0 \\ 0 & 0 & J_3 \end{pmatrix} \begin{pmatrix} \ddot{\delta}_{x_h} \\ \ddot{\delta}_2 \\ \ddot{\delta}_3 \end{pmatrix} + \begin{pmatrix} c_{v,x_h} & 0 & 0 \\ 0 & c_{v,2} & 0 \\ 0 & 0 & c_{v,3} \end{pmatrix} \begin{pmatrix} \dot{\delta}_{x_h} \\ \dot{\delta}_2 \\ \dot{\delta}_3 \end{pmatrix} + \begin{pmatrix} k_{x_h} & 0 & 0 \\ 0 & k_2 & 0 \\ 0 & 0 & k_3 \end{pmatrix} \begin{pmatrix} \delta_{x_h} \\ \delta_2 \\ \delta_3 \end{pmatrix} = \begin{pmatrix} M_{x_h} \\ M_2 \\ M_3 \end{pmatrix} \tag{18}$$

As Eq. (18) clarifies, the equations of motion about the AORs are uncoupled and the mean and dynamic response can be modeled according to Eq. (14) with axes $ax = x_h, 2, 3$. However, the modeled response about the AORs is not equal to the desired tracking deviations which are defined about the concentrator axes. Therefore, the response has to be transformed from the AORs to the concentrator axes which, in case of the mean component, leads to the following description:

$$\begin{pmatrix} \overline{\delta}_{x_h} \\ \overline{\delta}_{y_h} \\ \overline{\delta}_{z_h} \end{pmatrix} = \begin{pmatrix} k^*_{x_h} & 0 & 0 \\ 0 & k^*_2 \cos^2\theta + k^*_3 \sin^2\theta & (k^*_2 - k^*_3)\sin\theta\cos\theta \\ 0 & (k^*_2 - k^*_3)\sin\theta\cos\theta & k^*_3 \cos^2\theta + k^*_2 \sin^2\theta \end{pmatrix} \begin{pmatrix} \overline{M}_{x_h} \\ \overline{M}_{y_h} \\ \overline{M}_{z_h} \end{pmatrix} \tag{19}$$

From Eq. (19), it becomes apparent that modeling the response about the concentrator y_h- and z_h-axis is rather complex. The complexity significantly reduces if the inverse stiffnesses k^*_2 and k^*_3 can be assumed approximately equal. However, this assumption may not be universally applicable but must be evaluated for each specific heliostat. Therefore, the complete, yet complex description of Eq. (19) is kept. Finally, the mean wind-induced tracking deviations can be derived from Eq. (19) when taking into account that no significant moment about the z_h-axis is induced by the natural wind due to the small area exposed to the wind. With $\overline{M}_{z_h} \approx 0$, the mean wind-induced tracking deviations read

$$\begin{pmatrix} \overline{\delta}_{x_h} \\ \overline{\delta}_{y_h} \end{pmatrix} = \begin{pmatrix} k^*_{x_h} & 0 \\ 0 & k^*_2 \cos^2\theta + k^*_3 \sin^2\theta \end{pmatrix} \begin{pmatrix} \overline{M}_{x_h} \\ \overline{M}_{y_h} \end{pmatrix} \tag{20}$$

Similarly, the dynamic wind-induced tracking deviations can be derived and their amplitudes are modeled by

$$\begin{pmatrix} \widehat{\delta'}_{x_h} \\ \widehat{\delta'}_{y_h} \end{pmatrix} = \begin{pmatrix} k^*_{x_h} \chi_{m,x_h}(f) & 0 \\ 0 & k^*_2 \chi_{m,2}(f)\cos^2\theta + k^*_3 \chi_{m,3}(f)\sin^2\theta \end{pmatrix} \begin{pmatrix} \widehat{M'}_{x_h} \\ \widehat{M'}_{y_h} \end{pmatrix} \tag{21}$$

Lastly, the dynamic tracking deviations can be described in frequency domain in terms of their power spectral densities as follows:

$$\begin{pmatrix} S_{\delta_{xh}}(f) \\ S_{\delta_{yh}}(f) \end{pmatrix} = \begin{pmatrix} \left(k^*_{x_h} \chi_{m,x_h}\right)^2 & 0 \\ 0 & \left(k^*_2 \chi_{m,2}\cos^2\theta + k^*_3 \chi_{m,3}\sin^2\theta\right)^2 \end{pmatrix} \begin{pmatrix} S_{M_{xh}} \\ S_{M_{yh}} \end{pmatrix} \tag{22}$$

In conclusion, for a T-type heliostat with a pylon mounted gear drive and a linear actuator, the mean and dynamic wind-induced tracking deviations can be modeled according to Eqs. (20) and (22).

3.2. Stellio type heliostat

A Stellio type heliostat has a pentagonal shaped concentrator and is equipped with two inclined linear actuators. Fig. 10 shows a 48.5 m^2 Stellio heliostat, developed by sbp sonne GmbH together with Masermic and Ingemetal. Note that for these types of heliostats, due to the inclined linear actuators and their associated tracking axes, the rotational alignment of the concentrator changes with varying heliostat orientations (i.e. a certain combination of elevation an azimuth angle). In other terms, the concentrator appears to be rotated about the z_h-axis when changing the heliostat's azimuth or elevation angle. Therefore, certain structural axes and (partly) the tracking axes can change orientation while the orientation of the concentrator axes x_h (defined horizontally) and y_h (defined vertically in the plane of the concentrator) remains unchanged. Due to that, the concentrator axes are not necessarily equal to the AORs which are, as previously stated, often considered to be equal to the tracking axes. Hence, the model representation must be adjusted.

For completeness, the following note shall be given regarding the AORs of a Stellio type heliostat. In particular for large- to mid-size Stellio type heliostats as the one shown in Fig. 10, the entire drive system is comparably small (in relation to the concentrator) and may also be imagined as a large ball joint which does not have dominant tracking axes but is, in principle, able to rotate in any direction. Then, depending on the specific orientation of the concentrator and its rotational alignment, certain symmetry axes may also represent the AORs rather than the tracking axes. This aspect is further analyzed in Section 4.2.2.

Following the approach that the tracking axes determine the AORs, Fig. 6 shows a schematic of the mass–spring–damper system where the black axes represent the concentrator axes (x_h, y_h, z_h) while the red axes represent one possible orientation of the tracking axes, i.e. the AORs $(1, 2, z_h)$. For the Stellio type heliostat, the rotatable part of the system is considered to be the concentrator only and the principle axes of inertia can be assumed to approximately coincide with the AORs. The equations of motion about the AORs then read in matrix notation:

$$\begin{pmatrix} J_1 & 0 & 0 \\ 0 & J_2 & 0 \\ 0 & 0 & J_{z_h} \end{pmatrix} \begin{pmatrix} \ddot{\delta}_1 \\ \ddot{\delta}_2 \\ \ddot{\delta}_{z_h} \end{pmatrix} + \begin{pmatrix} c_{v,1} & 0 & 0 \\ 0 & c_{v,2} & 0 \\ 0 & 0 & c_{v,z_h} \end{pmatrix} \begin{pmatrix} \dot{\delta}_1 \\ \dot{\delta}_2 \\ \dot{\delta}_{z_h} \end{pmatrix} + \begin{pmatrix} k_1 & 0 & 0 \\ 0 & k_2 & 0 \\ 0 & 0 & k_{z_h} \end{pmatrix} \begin{pmatrix} \delta_1 \\ \delta_2 \\ \delta_{z_h} \end{pmatrix} = \begin{pmatrix} M_1 \\ M_2 \\ M_{z_h} \end{pmatrix} \tag{23}$$

Eq. (23) again clarifies that the equations of motion about the AORs are uncoupled and the mean and dynamic response can be modeled according to Eq. (14) with axes $ax = 1, 2, z_h$. By transforming the modeled response from the AORs to the concentrator axes, the mean and dynamic wind-induced tracking deviations can be derived. The mean tracking deviations are described by

$$\begin{aligned} \begin{pmatrix} \overline{\delta}_{x_h} \\ \overline{\delta}_{y_h} \end{pmatrix} &= \begin{pmatrix} k^*_1 \cos^2\theta + k^*_2 \sin^2\theta & (k^*_1 - k^*_2)\sin\theta\cos\theta \\ (k^*_1 - k^*_2)\sin\theta\cos\theta & k^*_2 \cos^2\theta + k^*_1 \sin^2\theta \end{pmatrix} \begin{pmatrix} \overline{M}_{x_h} \\ \overline{M}_{y_h} \end{pmatrix} \\ &= \begin{pmatrix} k^*_1 & 0 \\ 0 & k^*_2 \end{pmatrix} \begin{pmatrix} \cos^2\theta + \frac{1}{C}\sin^2\theta & (1 - \frac{1}{C})\sin\theta\cos\theta \\ (C-1)\sin\theta\cos\theta & \cos^2\theta + C\sin^2\theta \end{pmatrix} \begin{pmatrix} \overline{M}_{x_h} \\ \overline{M}_{y_h} \end{pmatrix} \end{aligned} \tag{24}$$

in which the variable $C = k^*_1/k^*_2$ defines the ratio of the inverse concentrator stiffnesses. Furthermore, the amplitudes of the dynamic tracking deviations are described in Box I, where the variables a_1 to a_4 replace the matrix entries.

$$\begin{aligned}\begin{pmatrix}\widehat{\delta}'_{x_h}\\ \widehat{\delta}'_{y_h}\end{pmatrix} &= \begin{pmatrix}k_1^*\chi_{m,1}\cos^2\theta + k_2^*\chi_{m,2}\sin^2\theta & (k_1^*\chi_{m,1} - k_2^*\chi_{m,2})\sin\theta\cos\theta\\ (k_1^*\chi_{m,1} - k_2^*\chi_{m,2})\sin\theta\cos\theta & k_2^*\chi_{m,2}\cos^2\theta + k_1^*\chi_{m,1}\sin^2\theta\end{pmatrix}\begin{pmatrix}\widehat{M}'_{x_h}\\ \widehat{M}'_{y_h}\end{pmatrix}\\ &= \begin{pmatrix}k_1^* & 0\\ 0 & k_2^*\end{pmatrix}\begin{pmatrix}\chi_{m,1}\cos^2\theta + \frac{1}{C}\chi_{m,2}\sin^2\theta & (\chi_{m,1} - \frac{1}{C}\chi_{m,2})\sin\theta\cos\theta\\ (C\chi_{m,1} - \chi_{m,2})\sin\theta\cos\theta & \chi_{m,2}\cos^2\theta + C\chi_{m,1}\sin^2\theta\end{pmatrix}\begin{pmatrix}\widehat{M}'_{x_h}\\ \widehat{M}'_{y_h}\end{pmatrix}\\ &= \begin{pmatrix}k_1^* & 0\\ 0 & k_2^*\end{pmatrix}\begin{pmatrix}a_1 & a_2\\ a_3 & a_4\end{pmatrix}\begin{pmatrix}\widehat{M}'_{x_h}\\ \widehat{M}'_{y_h}\end{pmatrix}\end{aligned} \tag{25}$$

Box I.

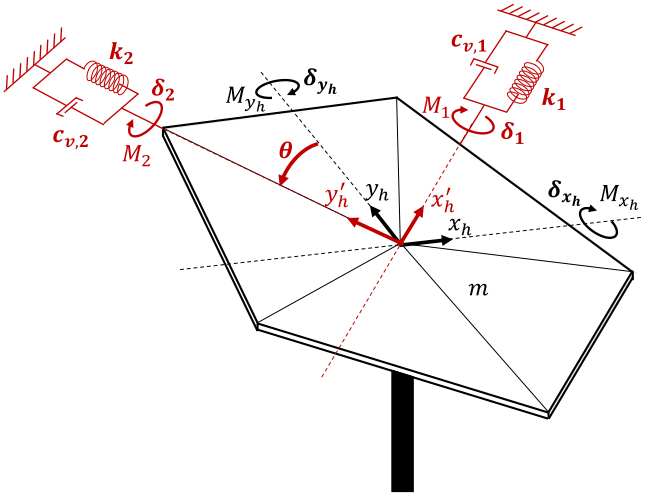

Fig. 6. Schematic of the mass–spring–damper system of a Stellio type heliostat. One possible orientation of the expected axes of rotation system is shown in red which is rotated about the z_h-axis compared to the concentrator axes system (black). (For interpretation of the references to color in this figure legend, the reader is referred to the web version of this article.)

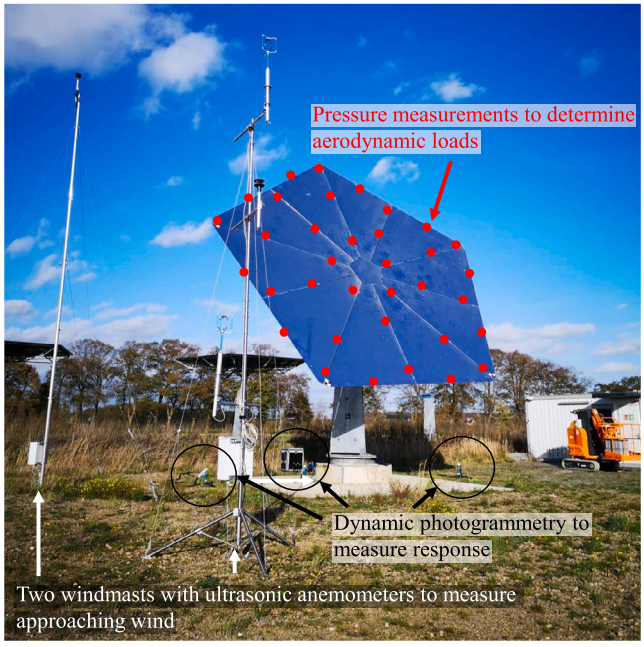

Fig. 7. Principal measurement setup of the field study, exemplarily shown for the Stellio heliostat.

Lastly, the dynamic tracking deviations must be described in frequency domain in terms of the power spectral densities. Under consideration of the abbreviated matrix entries a_1 to a_4, the power spectral densities can be described by

$$\begin{pmatrix}S_{\delta_{xh}}\\ S_{\delta_{yh}}\end{pmatrix} = \begin{pmatrix}(a_1k_1^*)^2 & 2a_1a_2(k_1^*)^2 & (a_2k_1^*)^2\\ (a_3k_2^*)^2 & 2a_3a_4(k_2^*)^2 & (a_4k_2^*)^2\end{pmatrix}\begin{pmatrix}S_{M_{xh}}\\ S_{M_{xh}M_{yh}}\\ S_{M_{yh}}\end{pmatrix} \tag{26}$$

in which $S_{M_{xh}}$ and $S_{M_{yh}}$ denote the power spectral densities, i.e. the spectra of the respective moments while $S_{M_{xh}M_{yh}}$ represents the co-spectrum of the fluctuating aerodynamic moments M'_{x_h} and M'_{y_h}. In conclusion, for a Stellio type heliostat, the mean and dynamic wind-induced tracking deviations can be modeled according to Eqs. (24) and (26). Note that in case of Stellio type heliostats, due to the application of two similar or equal linear actuators, it is often reasonable to assume that the (inverse) concentrator stiffness is approximately equal in any direction, i.e. $k_1^* \approx k_2^*$ and thus $C \approx 1$ which simplifies the model representation.

4. Application and verification of analytical model

The developed analytical model can be verified by applying it to measurement data of a field study and by comparing its predicted behavior to the true behavior of a full-scale heliostat. Therefore, a field study was conducted at a Stellio and a HelFer (T-type) heliostat at the DLR site in Juelich. During the field study, the approaching wind, the pressure distribution over the heliostat's concentrator to determine the acting aerodynamic load and the heliostat's response was measured simultaneously. In Fig. 7, the principal measurement setup of the field study is exemplarily shown for the Stellio heliostat. The data of the field study can then be used to analyze the aerodynamic and the structural side of the developed model representation which will be discussed in the following Sections 4.1 and 4.2. Note that this paper cannot present all details of the field study and will therefore, where appropriate, refer to dedicated publications.

4.1. Aerodynamic side

The aerodynamic side of the model representation is investigated by applying the wind and load data of the field study to the model representation. Note that the scope of the field study was not limited to investigating the aerodynamic moments but took the aerodynamic lift and drag forces into account as well. For the drag and lift forces, the developed model applies accordingly. Therefore, the general term load is used in the following. The load data was evaluated only for the Stellio heliostat but not for the HelFer and the investigation of the aerodynamic side is therefore based on the Stellio results only. At this point, it shall be outlined that the Stellio wind and pressure measurements are presented in much more detail in the dedicated publication Blume et al. (2023) where also the evaluation of the data and its application to the model representation is discussed in more

detail. Therefore, only a brief summary of the measurement procedure and the main conclusions will be given in the following while it is referred to Blume et al. (2023) for a detailed discussion.

During the field study, individual 10-minute measurement periods were conducted during which the approaching wind was measured through ultrasonic anemometers that were attached to two wind masts in front of the Stellio as indicated in Fig. 7. Moreover, the aerodynamic loads were determined through pressure measurements over the Stellio's concentrator. The measured pressure distributions were integrated over the surface to evaluate the aerodynamic loads which acted on the entire concentrator. While for each measurement period the mean horizontal angle of attack $\overline{\beta}$ varied according to the approaching wind, the elevation angle, i.e. the mean vertical angle of attack was fixed to $\overline{\alpha} = 60°$.

The wind and load data is then applied to the developed model to analyze its applicability. As a short recapitulation of Section 2.1, the aerodynamic side of the model accounts for a mean and a dynamic load component. The mean load component is modeled through the non-dimensional mean load coefficient (see Eq. (9)) while the dynamic component is modeled through the wind spectra and the aerodynamic admittance function (see Eq. (10)). To fully analyze the developed model representation, the field study data is evaluated in two ways. (1) First, the mean non-dimensional load coefficients are calculated and presented over the mean angles of attack which gives insight into the modeling of the mean component. (2) Second, the aerodynamic admittance function is calculated for all load components which gives particular insight into the dynamic component. The main findings and conclusions regarding the model applicability can be summarized as follows. Again note that a detailed discussion and graphs of the results are presented in Blume et al. (2023).

Ad (1): The calculation of the mean load component through the non-dimensional mean load coefficients is a well known and accepted method. Therefore, no abnormalities are expected when applying the field study data to the model representation and in fact, the evaluated courses of the mean load coefficients over the mean angles of attack agree well with the expectations. Hence, the mean loads can be considered well evaluable through the developed model if load coefficients are available. The load coefficients presented in Blume et al. (2023) for the Stellio heliostat can be used as a first set of coefficients.

Ad (2): The dynamic component of the model representation is analyzed through the aerodynamic admittance function which, based on Eq. (10), can be calculated by

$$|\chi_{a,L}(f)|^2 = \frac{\overline{u}^2 S_{c_L}(f)}{4\overline{c}_L^2 S_u(f) + (\frac{\partial c_L}{\partial \beta})^2 \ S_v(f) + (\frac{\partial c_L}{\partial \alpha})^2 \ S_w(f)} \tag{27}$$

in which L represents the desired aerodynamic load component. From Eq. (27), the admittance functions are then calculated by applying the wind and load data of each individual measurement period. In more detail, the admittance functions of the drag force and of the moment about the y_h-axis are fully evaluable based on the available field study data. For both load components, the calculated admittances agree well with the expectations, i.e. the admittances tend towards unity for small frequencies and decrease for larger frequencies. Moreover, the calculated admittances of the drag force agree well with a reference case, the widely known Vickery admittance function which was determined by Vickery (1965) through wind tunnel measurements. On a last note, it shall be outlined that the developed aerodynamic admittance model (Eq. (27)) is in accordance with a calculation model that Jafari et al. (2019) used to evaluate wind tunnel data of a heliostat who in turn adopted the model from Larose and Livesey (1997). The specific investigation case in these studies was the lift force (F_L) on a horizontal flat plate or heliostat. For this investigation case, the derivative $\frac{\partial c_{F_L}}{\partial \beta}$ is negligible compared to $\frac{\partial c_{F_L}}{\partial \alpha}$. Neglecting the $\frac{\partial c_{F_L}}{\partial \beta}$-related term in Eq. (27) results in the same calculation model as given by Larose and Livesey (1997) and adopted by Jafari et al. (2019).

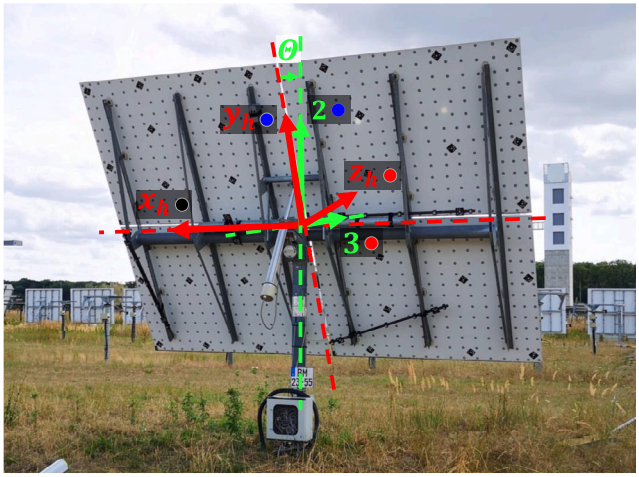

Fig. 8. Expected axes of rotation (green) and concentrator axes (red) of the HelFer heliostat. Angle of rotation θ is 30°. Dot colors next to axis labels correspond to line colors in Fig. 9. (For interpretation of the references to color in this figure legend, the reader is referred to the web version of this article.)

Moreover, Jafari et al. (2019) applied such model to the data of the heliostat wind tunnel study and the results agreed well with the expectations, thus the model was well applicable.

In conclusion, the application of the developed aerodynamic model to measurement data of a field study, as well as the comparison of the developed model to reference models found in literature was successful and supported the developed model. It is therefore considered a well suitable model to estimate wind loads on heliostats. At the same time, it is clearly a simplified model; to determine loads with highest accuracy, more complex methods have to be applied.

4.2. Structural side

The structural side of the model representation can be analyzed based on the dynamic photogrammetry measurements, i.e. the response measurements of the heliostats. Through a dynamic photogrammetry measurement, the motion of the concentrator is captured and can be translated into the wind-induced deviations about arbitrary axes. By evaluating the wind-induced deviations about the concentrator axes and about the expected AORs, the applicability of the model representation and the underlying assumptions can be investigated. This is presented in the following Sections 4.2.1 and 4.2.2 for the HelFer and the Stellio heliostat.

4.2.1. HelFer heliostat

As explained in Section 3.1, the AORs of a HelFer type heliostat are considered to be approximately equal to the concentrator x_h-axis, the pylon axis (axis 2) and such axis that horizontally points away from the heliostat (axis 3). Compared to the concentrator axes (x_h, y_h, z_h), the AORs $(x_h, 2, 3)$ are thus rotated about the x_h-axis according to the elevation angle. Fig. 8 shows a picture of the HelFer heliostat as installed in Juelich and depicts the concentrator axes in red as well as the expected AORs in green. Note that the x-axis of the green system is equivalent to the concentrator x_h-axis and is not additionally depicted in green. The colored dots next to the axis labels correspond to the line colors in Fig. 9 where the power spectral densities, i.e. the spectra of the wind-induced deviations are presented that were measured through the dynamic photogrammetry system. To analyze the developed model representation, the measured wind-induced deviations can be expressed about either of the aforementioned axes, i.e. the concentrator axes and the AORs. Therefore, Figs. 9(a) and 9(b) show the spectra of the deviations when being evaluated about the concentrator axes and

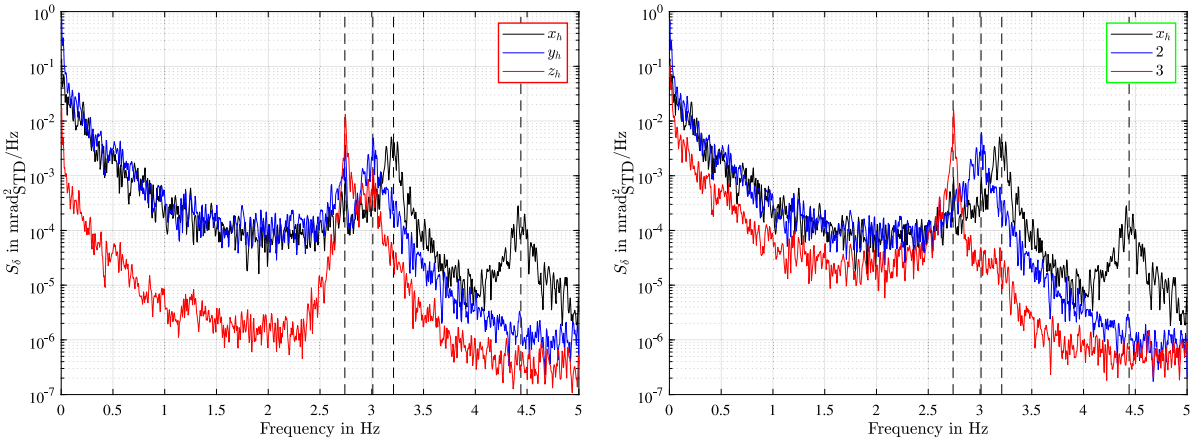

(a) Evaluated about the concentrator axes (red axes in figure 8). (b) Evaluated about the expected axes of rotation (green axes in figure 8).

Fig. 9. Power spectral densities, i.e. spectra of measured wind-induced deviations of the HelFer heliostat. Dashed lines indicate the positions of the peaks and correspond to the excited eigenfrequencies.

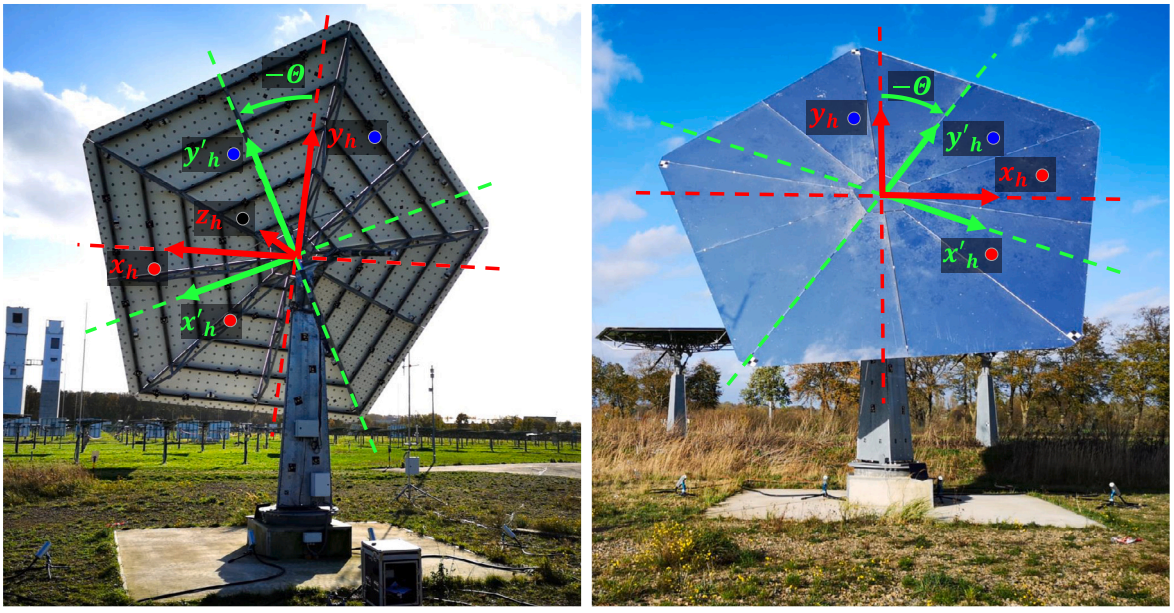

(a) Back view. (b) Front view.

Fig. 10. Stellio concentrator axes (red) and approximate tracking axes (green). Both the red and green axes can potentially represent the Stellio's axes of rotation. Angle of rotation $|\theta|$ is 32° for the depicted Stellio position. Dot colors next to axis labels correspond to line colors in Fig. 11. (For interpretation of the references to color in this figure legend, the reader is referred to the web version of this article.)

about the AORs. In the following, the spectra of the wind-induced deviations are also simply referred to as the response spectra. The peaks which become apparent in the response spectra in Figs. 9(a) and 9(b) correspond to the excited eigenfrequencies of the HelFer heliostat and characterize its dynamic response. This true dynamic behavior can be compared to the developed model representation for verification.

Based on the underlying assumptions of the developed model, in particular the assumption of a rigid pylon, the model predicts the following heliostat behavior. Under (wind) load, the heliostat's concentrator will rotate about its three AORs where one approximate rigid body mode, i.e. one eigenfrequency, will contribute to the rotation about each AOR. Therefore, when evaluating the heliostat's response in frequency domain, as shown in Fig. 9, it is expected that each of the three response spectra reveals one single peak if the response is evaluated about the AORs. Considering these explanations, two aspects become apparent when analyzing Figs. 9(a) and 9(b).

First, a comparison of both figures shows that the peaks in Fig. 9(b) are well separated while in Fig. 9(a) the peaks of the blue and red spectra overlap and blur. Hence, the heliostat's response about the y_h- and z_h-axis is coupled which indicates that the concentrator axes are not identical to the AORs, as was expected. In turn, the well separated peaks in Fig. 9(b) indicate that the response is uncoupled and that the AORs were predicted correctly.

Second, it becomes apparent from Fig. 9(b) that not only three peaks are present, as expected, but in total four peaks arise. In more detail, the black spectrum which represents the wind-induced deviations about

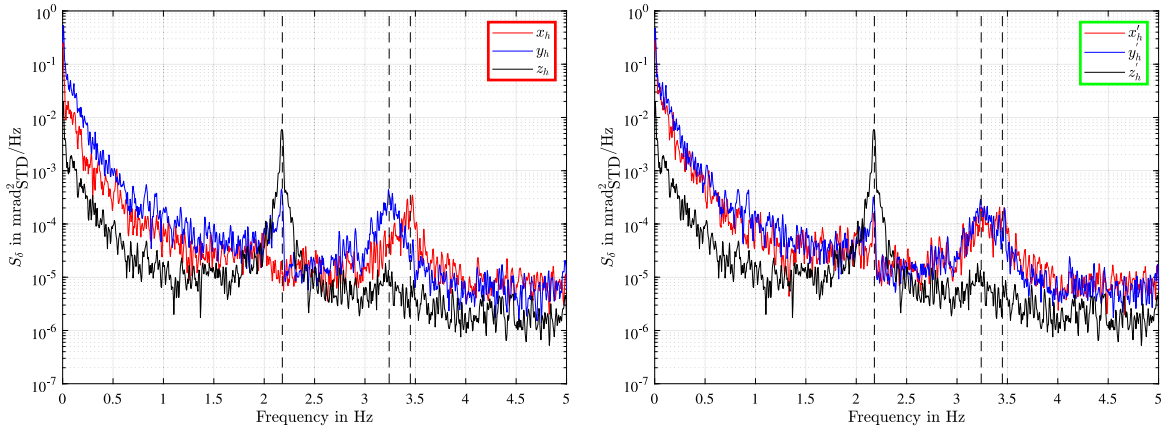

(a) Evaluated about the concentrator axes, i.e. the red axes in figure 10.

(b) Evaluated about the approximate tracking axes, i.e. the green axes in figure 10.

Fig. 11. Power spectral densities, i.e. spectra of measured wind-induced deviations of the Stellio heliostat. Dashed lines indicate the positions of the peaks and correspond to the excited eigenfrequencies. (For interpretation of the references to color in this figure legend, the reader is referred to the web version of this article.)

the concentrator x_h-axis reveals two peaks instead of a single peak. This behavior is in contradiction with the model representation and is due to the fact that the assumption of a rigid pylon is violated in case of the HelFer heliostat. The HelFer as installed in Juelich is a prototype and the rigidity of the pylon was not optimized for the specific concentrator. Therefore, the wind load does not only excite rigid body modes of the concentrator but also bending modes of the pylon. These interact with the concentrator rigid body modes and lead to the appearance of two eigenfrequencies within the black spectrum in Fig. 9. Such interaction and the excitation of pylon bending modes is not covered by the model representation at the current stage of development. Yet, the structural side of the model representation can be extended and adjusted in future. Moreover, it shall be outlined that further investigations showed that the first black peak in Fig. 9 is the major contributor to the response about the x_h-axis while the second black peak has no significant impact. This indicates that modeling only the first peak and its corresponding eigenfrequency is sufficient while the second one can be neglected. In this case, the developed model representation can be applied.

4.2.2. Stellio heliostat

In contrast to the HelFer heliostat, the Stellio as installed in Juelich is considered to have a sufficiently rigid pylon. Thus, the Stellio is expected to behave as predicted by the model representation. This can again be analyzed by evaluating the measured wind-induced deviations in frequency domain. Prior to that, the AORs must be discussed. Fig. 10 shows the Stellio as installed in Juelich and, more precisely, shows the exact orientation which was applied during the response measurements. As explained in Section 3.2, the AORs of a Stellio type heliostat can (but may not always) correspond to the tracking axes which are therefore indicated in green in Fig. 10. Besides, when considering the absence of dominant tracking axes, i.e. imagining the connection of the concentrator to the pylon through a large ball joint, other structural axes can as well represent the AORs. As becomes apparent from Fig. 10, for the specific here investigated Stellio orientation, the concentrator y_h-axis is approximately equal to the concentrator's symmetry axis. Therefore, the red concentrator axes as shown in Fig. 10 may also represent the AORs. To investigate this further, the measured wind-induced deviations have been evaluated about the red and the green axes and the response spectra are shown in Fig. 10 where the peaks correspond to the eigenfrequencies of the Stellio. From these results, the following two conclusions can be drawn.

First, a comparison of the red and blue spectra in Figs. 11(a) and 11(b) reveals that the red axes are better estimations of the AORs than the green (tracking) axes. While in Fig. 11(b) the blue and red peak notably overlap and blur, the peaks are well separated in Fig. 11(a) which indicates that the response about the x_h- and y_h-axis is uncoupled. Consequently, the red axes in Fig. 10 are better approximations of the AORs than the green axes. Note that the red axes still do not represent the AORs perfectly but only approximately because a minor coupling remains between the y_h- and z_h-axis as becomes apparent from Fig. 11(a). In Fig. 11(a), the black peak is accompanied by a minor blue peak which indicates that the response is coupled and that the true AORs are rotated about the x_h-axis compared to the red axes. However, further investigations showed that the rotation angle between the true AORs and the red axes is approximately 10° and thus rather small. Hence, the red axes are good approximations of the AORs.

By analyzing the spectra of the (approximately) uncoupled wind-induced deviations in Fig. 11(a), the following second conclusion can be drawn. In contrast to the results of the HelFer heliostat and the appearance of four eigenfrequencies, Fig. 11(a) shows that in case of the Stellio only three peaks arise. These three eigenfrequencies can be assigned to the three predicted approximate rigid body modes about the three AORs. Hence, in case of the Stellio for which the assumption of a rigid pylon holds, the model representation predicts the heliostat behavior correctly.

In conclusion, the response of both investigated heliostats is well explainable through the developed model representation. Even though the HelFer response differs slightly from the predicted behavior, such difference does not indicate an inconsistency of the developed model but is due to the non-applicability of one of the model assumptions. Hence, when using the model it must be assured that all model assumptions apply to the heliostat under investigation.

5. Workflow and input parameters to use analytical model

The developed analytical model allows to estimate and predict wind loads and wind-induced tracking deviations of heliostats based on only few input parameters. To maximize the practical usability of the model, the input parameters shall be easy-to-determine and the following workflow is suggested to derive the necessary input parameters:

- The mean wind speed and the air density can be chosen freely.
- The wind spectra can either be taken from wind measurements or can be calculated from model representations that are available in pertinent literature.
- The mean moment coefficients and their courses over the angles of attack as well as the aerodynamic admittance function can for

example be taken from commonly available wind tunnel studies or from full-scale studies such as Blume et al. (2023).
- The geometric parameters of the heliostat, i.e. the concentrator area and a characteristic length are either available from construction drawings or can be easily measured at the full-scale heliostat.
- The mechanical parameters of the heliostat, i.e. the concentrator stiffness, the eigenfrequencies and the damping ratios are presumably the least available parameters for a certain heliostat. However, through a relatively simple experimental procedure at the full-scale heliostat, the parameters can be determined. The experimental procedure is a pulling test during which the concentrator must be gradually deviated by applying a known force while at the same time measuring the concentrator deviation. From this data the concentrator stiffness can be evaluated. Once the concentrator is deviated to a certain extent, the applied force can be released and the concentrator oscillates freely in a damped manner. By measuring such oscillation, the eigenfrequencies and damping ratios can be evaluated. The detailed procedure of the pulling test and recommendations on the correct procedure will be published in future.

6. Summary and conclusion

In this study, the development of a simplified analytical model to describe wind loads and wind-induced tracking deviations of heliostats was presented. The development process was described in detail to clarify the necessary simplifications and assumptions. More specifically, the model was developed for an isolated heliostat subject to the natural wind. An application to heliostat fields is potentially possible, but future investigations are necessary to evaluate the validity of the simplifications applied. As the model was derived for a relatively simple heliostat type, an adjustment of the model to more complex types was exemplarily explained for a pentagonal heliostat with two inclined linear actuators (Stellio type heliostat) and a rectangular heliostat with a pylon mounted gear drive and a linear actuator (T-type heliostat). Based on these explanations, further adjustments to other types of heliostats can be performed in future. For verification purposes, the developed model was then applied to measurement data of a field study. The results agreed well with the expectations and it was shown that the measured heliostat response matched the predicted response well, provided the underlying assumptions of the model fully applied to the investigated heliostat. Overall, no unexplainable inconsistencies were identified and the results supported the developed model well. A further validation of the model can be performed in future by comparing modeled and measured wind-induced tracking deviations. This investigation has not been presented in this paper but will be part of future publications. Finally, for the practical use of the developed analytical model, the workflow and the determination of the necessary input parameters was summarized. In particular, it was pointed out that the input parameters are easily determinable by using commonly available wind spectrum data from literature, known geometry data of the heliostat, commonly available results of wind-tunnel or full-scale studies, and a pulling test.

In conclusion, through the developed analytical model, a method is provided to estimate and predict wind loads and tracking deviations of different types of heliostats based on only a few and easy-to-determine input parameters. At the same time, it is a simplified model suitable to estimate aforementioned parameters; to achieve results with highest accuracy, more complex methods must be applied. Also, the developed model is inevitably based on assumptions and simplifications which can potentially limit its applicability (e.g. a so far unclear applicability to heliostat fields). Yet, the application of a simplified model is often sufficient, e.g. to compare the tracking performance of different types of heliostats under wind or to identify those parameters that have the greatest impact on the wind-induced tracking deviations.

Declaration of competing interest

The authors declare that they have no known competing financial interests or personal relationships that could have appeared to influence the work reported in this paper.

Acknowledgments

The authors gratefully acknowledge the financial support of the German Federal Ministry for Economic Affairs and Climate Action, Germany (Heliodor contract 0324310). The authors would furthermore like to thank the companies sbp sonne GmbH and Kraftanlagen Energies & Services GmbH for providing the Stellio and the HelFer heliostat, respectively. Finally, the authors would like to thank the anonymous reviewers for their valuable comments to the manuscript.

References

Baker, C.J., Jones, J., Lopez-Calleja, F., Munday, J., 2004. Measurements of the cross wind forces on trains. J. Wind Eng. Ind. Aerodyn. 92, 547–563. http://dx.doi.org/10.1016/j.jweia.2004.03.002.

Blume, K., Röger, M., Pitz-Paal, R., 2023. Full-scale investigation of heliostat aerodynamics through wind and pressure measurements at a pentagonal heliostat. Sol. Energy 251, 337–349. http://dx.doi.org/10.1016/j.solener.2022.12.016.

Blume, K., Röger, M., Schlichting, T., Macke, A., Pitz-Paal, R., 2020. Dynamic photogrammetry applied to a real scale heliostat: Insights into the wind-induced behavior and effects on the optical performance. Sol. Energy 212, 297–308. http://dx.doi.org/10.1016/j.solener.2020.10.056.

Davenport, A.G., 1961. The application of statistical concepts to the wind loading of structures. Proc. Inst. Civ. Eng. 19, 449–472. http://dx.doi.org/10.1680/iicep.1961.11304.

Davenport, A.G., 1964. The buffeting of large superficial structures by atmospheric turbulence. Ann. New York Acad. Sci. 116, 135–160. http://dx.doi.org/10.1111/j.1749-6632.1964.tb33943.x.

Davenport, A.G., 1967. Tall buildings. In: Smith, A.C., Stafford, B. (Eds.), The Treatment of Wind Loading on Tall Buildings. Pergamon, pp. 3–45. http://dx.doi.org/10.1016/b978-0-08-011692-1.50006-7.

Dyrbye, C., Hansen, S.O., 1999. Wind Loads on Structures. Wiley, Chichester, England.

Emes, M.J., Jafari, A., Ghanadi, F., Arjomandi, M., 2019. Hinge and overturning moments due to unsteady heliostat pressure distributions in a turbulent atmospheric boundary layer. Sol. Energy 193, 604–617. http://dx.doi.org/10.1016/j.solener.2019.09.097.

Emes, M.J., Jafari, A., Pfahl, A., Coventry, J., Arjomandi, M., 2021. A review of static and dynamic heliostat wind loads. Sol. Energy 225, 60–82. http://dx.doi.org/10.1016/j.solener.2021.07.014.

Heller, P., 2017. Introduction to CSP systems and performance. In: Heller, P. (Ed.), The Performance of Concentrated Solar Power (CSP) Systems. Woodhead Publishing, pp. 1–29. http://dx.doi.org/10.1016/B978-0-08-100447-0.00001-8.

Holmes, J.D., 2015. Wind Loading of Structures. Vol. 3, CRC Press, Boca Raton, USA, http://dx.doi.org/10.1201/b18029.

Jafari, A., Ghanadi, F., Emes, M.J., Arjomandi, M., Cazzolato, B.S., 2019. Measurement of unsteady wind loads in a wind tunnel: Scaling of turbulence spectra. J. Wind Eng. Ind. Aerodyn. 193, http://dx.doi.org/10.1016/j.jweia.2019.103955.

Kelly, S.G., 2012. Mechanical Vibrations: Theory and Applications, SI. Cengage Learning, Stamford, USA.

Larose, G.L., Livesey, F.M., 1997. Performance of streamlined bridge decks in relation to the aerodynamics of a flat plate. J. Wind Eng. Ind. Aerodyn. 69–71, 851–860. http://dx.doi.org/10.1016/S0167-6105(97)00211-0.

Petersen, C., Werkle, H., 2017. Dynamik der Baukonstruktionen. Vol. 2, Springer Vieweg, Wiesbaden, http://dx.doi.org/10.1007/978-3-8348-2109-6.

Quinn, A.D., Sterling, M., Robertson, A.P., Baker, C.J., 2007. An investigation of the wind-induced rolling moment on a commercial vehicle in the atmospheric boundary layer. Proc. Inst. Mech. Eng. D 221, 1367–1379. http://dx.doi.org/10.1243/09544070jauto537.

Röger, M., Blume, K., Schlichting, T., Collins, M., 2022. Status update of the SolarPACES heliostat testing activities. AIP Conf. Proc. 2445, 070010. http://dx.doi.org/10.1063/5.0087037.

Ruscheweyh, H., 1982. Dynamische Windwirkung an Bauwerken - Band 2: Praktische Anwendungen. Bauverlag, Wiesbaden, Berlin.

Sattler, J.C., Röger, M., Schwarzbözl, P., Buck, R., Macke, A., Raeder, C., Göttsche, J., 2020. Review of heliostat calibration and tracking control methods. Sol. Energy 207, 110–132. http://dx.doi.org/10.1016/j.solener.2020.06.030.

de Silva, C.W., 2005. Vibration and Shock Handbook, first ed. CRC Press, Boca Raton, USA, http://dx.doi.org/10.1201/9781420039894.

Stull, R.B., 1988. An Introduction to Boundary Layer Meteorology. Kluwer Academic, Dordrecht, Netherlands.

Teufel, E., Buck, R., Pfahl, A., Böing, G., Kunert, J., 2008. Dimensioning of heliostat components under wind and gravity load: the map approach. In: 14th Biennial CSP SolarPACES Symposium. Las Vegas, USA.

van der Hoven, I., 1957. Power spectrum of horizontal wind speed in the frequency range from 0.0007 to 900 cycles per hour. J. Meteorol. 14, http://dx.doi.org/10.1175/1520-0469(1957)014%3C0160:PSOHWS%3E2.0.CO;2.

Vásquez Arango, J.F., 2016. Dynamic wind loads on heliostats (Ph.D. thesis). Rheinisch-Westfälische Technische Hochschule Aachen, Aachen, Germany, http://dx.doi.org/10.18154/rwth-2016-12225.

Vickery, B.J., 1965. On the Flow Behind a Coarse Grid and Its Use as a Model of Atmospheric Turbulence in Studies Related to Wind Loads on Buildings. Report, National Physical Laboratory, Great Britain.